Progress In Electromagnetics Research M, Vol. 109, 163–177, 2022

High Power Density Spatial Combiner for the Q-Band, Ready for Space Applications

Stefano Fantauzzi*, Lorenzo Valletti, and Franco Di Paolo

Abstract—This paper outlines the design characterization and electromagnetic performance of a millimeter-wave high power combining structure, which exploits the spatial power combination technique. The input matching is always below 10 dB over the entire Q band, and the overall weight of the structure is about 500 g. Multiphysics simulations show how this structure is suitable for the most challenging space missions that will arise in next few years. In fact, 100 W of RF power above the frequency of 40 GHz can be delivered while all the specifications for satellite payloads are complied. Other Spatial Power Combiner structures, such as Radial ones, cannot be implemented in space missions since they are much less compact and much heavier than the one presented in this article, and this is the major advantage of this configuration which was specially designed for a space project.

1. INTRODUCTION

Spatial Power Combining techniques have become one of the most reliable and efficient techniques of millimeter-wave power combination. Reaching high powers in small volumes with high fault tolerances, Spatial Power Amplifiers (SPA) are the perfect candidates to replace high power Vacuum Tubes (VT) [1–12], especially in space environments. The only field in which vacuum tube technology remains unmatched is in the production of very high pulsed power [13]. Among all the disadvantages of Vacuum Tubes technology, including high bias voltages and heavy weight, the single point failure is the most critical one, especially in the case of space applications. Exploiting the Spatial Power Combining technique it is possible to merge the output power of several Solid State Power Amplifiers (SSPA) and so reaching the same RF power requirements as in the case of VTs, while offering the great advantage of solid state technology. Thanks to the reduced combining losses, the power density of the amplifier increases enormously, and the graceful degradation allows the device to continue operating while maintaining all the specifications and only reducing the output power, in great contrast to VTs single point failure. The very low losses introduced by the Spatial Power Combiner (SPC) structure are due to the way in which the dividing/combining operation is carried out, and for these architectures, a single stage parallel way power manipulation is involved, as depicted in Figure 1.

Moreover, in the case of waveguide systems, this operation is done in air, reducing losses even further thanks to the low dissipation factor. Many different electromagnetic field manipulation techniques performable inside a waveguide structure have been studied [14–17] also using polarizing systems [18]. A possible SPC division into families is reported in Figure 2.

In this article, a NON TEM, Single Waveguide, with Longitudinal Probes Spatial Power Combiner operating in Q band is presented, starting from the design of each millimeter-wave component and arriving at the measures performed on the manufactured device. In Fact, a sample structure, consisting in a back-to-back dividing/combining network, has been fabricated in order to validate the proposed spatial power combining technique. Furthermore, in terms of RF paths and mechanical structure, the

Received 9 December 2021, Accepted 15 February 2022, Scheduled 5 April 2022
* Corresponding author: Stefano Fantauzzi (stefano.fantauzzi@uniroma2.it).
The authors are with the Department of Electronic Engineering, University of Rome "Tor Vergata", Italy.

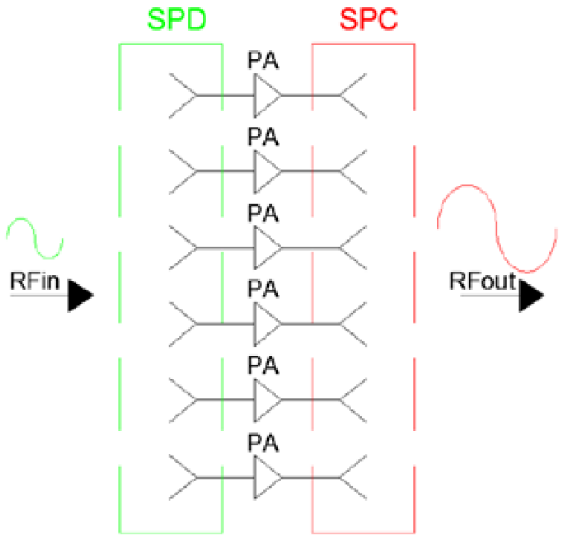

Figure 1. Single stage parallel power manipulation, the general concept of an SPC amplifier.

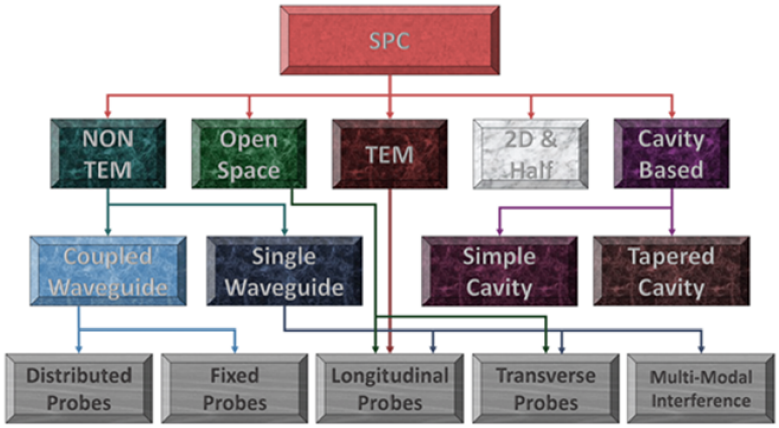

Figure 2. Spatial power combiners family.

combiner is ready to be enhanced with MMICs and becomes a significant high power density SPA. Dimensions and weight are two of the most important features in satellite applications which is why this architecture was chosen. The combining efficiency is not the maximum achievable with current systems, such as radial combiners [19–24], but the power-to-weight ratio and power density are definitely the best in literature up to this point, as shown in [8]. To conclude, multiphysics simulations certify the suitability of the system for space environments.

2. DESIGN

The Spatial Power Amplifier that can be realized starting from the passive structure proposed in this work operates in Q band, and it combines the power of 16 MMICs, 8 of which are placed on the top side and the other 8 on the bottom side. The SPC architecture chosen for the realization of the proposed prototype consists of an E-plane waveguide divider, realized in WR22 waveguide (for lower losses), and several waveguide to microstrips transitions, the latter implementing the Finline technology [25]. A final step of power division is made by a set of Wilkinson dividers placed right before the solid state power

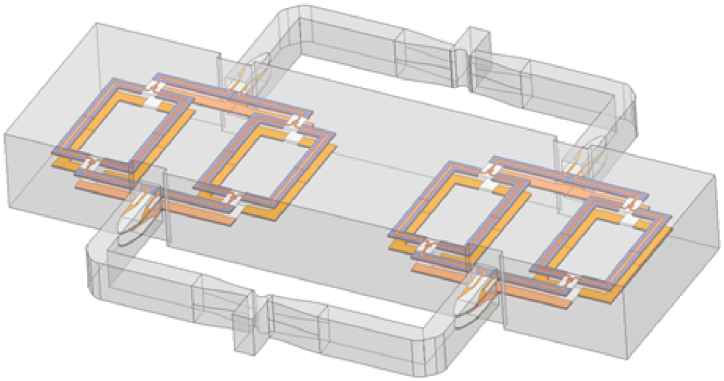

Figure 3. HFSS drawing of Q band SPC structure in back-to-back configuration, ready for EM simulations.

amplifiers. The drawing of the electromagnetic structure (Figure 3) was made in *HFSS* [26], along with the RF simulations.

The input power injected in the SPC is firstly divided by an E-plane T-junction made in WR22 waveguide, on the two branches of which a variation in the width of the waveguide walls has been made in order to accomplish the matching with the input port, thus realizing a Chebyshev taper.

After the Chebyshev transformer a 90° bend, for each branch of the T-Junction, was chamfered and optimized in depth to achieve the minimum return loss on the input side. Figure 4 reports this section.

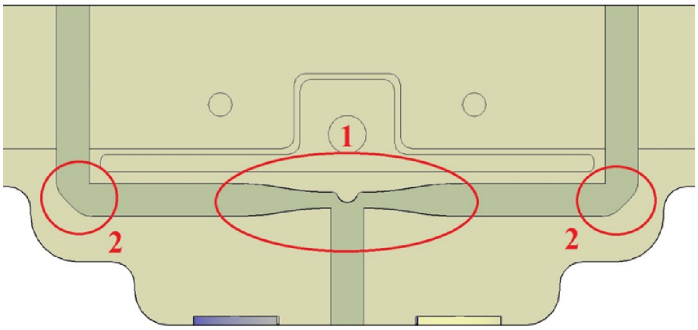

Figure 4. WR22 waveguide T-junction with Chebyshev transformer (1) and 90° bends with chamfers (2).

As for many other spatial combining architectures, dual finlines with exponential tapers made on Al_2O_3 substrate were adopted, in order to convey the traveling power from the waveguide into a planar power combining system. This conversion allows to implement the active devices which will be placed upon a copper carrier and fed by this RF power. The design equations for the finlines implemented are reported here:

$$\omega(z) = \omega_0 \left(e^{\left(\frac{z}{L}\ln(\omega_f)\right)} - 1 \right) \quad \omega_0 = \frac{\omega_{50} + \omega_{\text{sub}}}{2 \cdot (1 - \omega_f)} \tag{1}$$

where ω_0 represents the initial width of the taper; ω_f defines the curvature; L is the total length of the fin; ω_0 is composed by ω_{50}, the microstrip width, and ω_{sub}, the width of the substrate. Regarding this particular design, the values of each parameter are reported in Table 1.

Since the transition is placed inside the waveguide, its transversal height must be equal to the height of the chosen waveguide, in the case of a WR22, $b_{\text{WR22}} = 2.845\,\text{mm}$.

Table 1. Finline parameters.

Parameter	Value
ω_{sub}	1.778 mm
ω_f	0.15 mm
ω_{50}	0.25 mm
L	3.334 mm

Dual finlines in antipodal configuration completed by a quarter wave transition (QWT), which improves the input matching, can be depicted as shown in Figure 5.

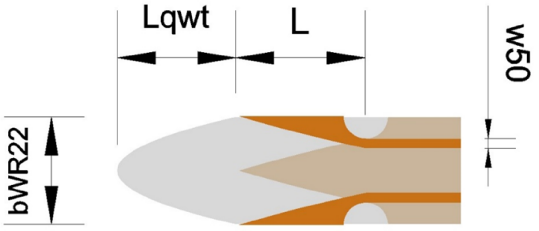

Figure 5. Dual finlines with quarter waveguide transformer.

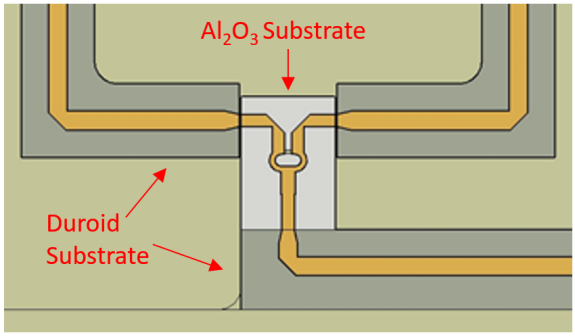

Figure 6. Wilkinson divider made on an Al_2O_3 substrate and microstrips lines made on RT/duroid 5880 substrate.

The antipodal configuration consists of two gold layers, one on the upper side of the dielectric substrate and one on the opposite side. As shown above, the profiles of these two layers are dual mirrored, and after the exponential taper part, they assume the shape of two adjacent microstrips sharing the same ground plane.

Continuing along the path of the traveling field, several Wilkinson dividers are realized on a 254 µm Al_2O_3 substrate (same as finlines), and these devices are fundamental in the perspective of graceful degradation. In fact, if any MMIC breaks, the system will continue to show an almost unchanged input impedance which is vital in the case of satellite payloads. Being in the range of millimeter-waves, the losses introduced by each additional section of microstrip can no longer be neglected. For this reason two different substrates were used for the realization of the planar section. The first is the aforementioned Al_2O_3 with a thickness of 254 µm while the second is Rogers RT/duroid 5880 with a thickness of 127 µm. The Duroid substrate has a lower insertion loss, thanks to both the lower tanδ and greater width of the gold microstrip, which allows to reduce ohmic losses. Thus, the interconnections among planar dividers, Wilkinson, and ginlines, are made by Duroid substrates, as it is possible to see in Figure 6, and this design choice is fundamental for reaching the maximum system efficiency.

From the output ports of the Wilkinson dividers, a microstrip line leads directly to the input pad of the solid state amplifiers, and from the output pad of the MMICs onwards, the very same input power dividing network is proposed again, in order to obtain an output power combining network with the same characteristics of the input one. A possible depiction of the final active structure can be seen in Figure 11. Since the structure proposed in this article is a passive back-to-back SPC, the only difference with the active Spatial Power Amplifier structure lies in the lack of MMICs, each of which is replaced by a microstrip line, and this absence leads to the structure shown in Figure 7.

All the millimeter-wave components mentioned before are glued on both sides of a copper carrier which is accommodated inside a mechanical frame made by two aluminium shells. The WR22 waveguide flange is embedded into the frame, providing greater robustness and greater compactness to the entire system.

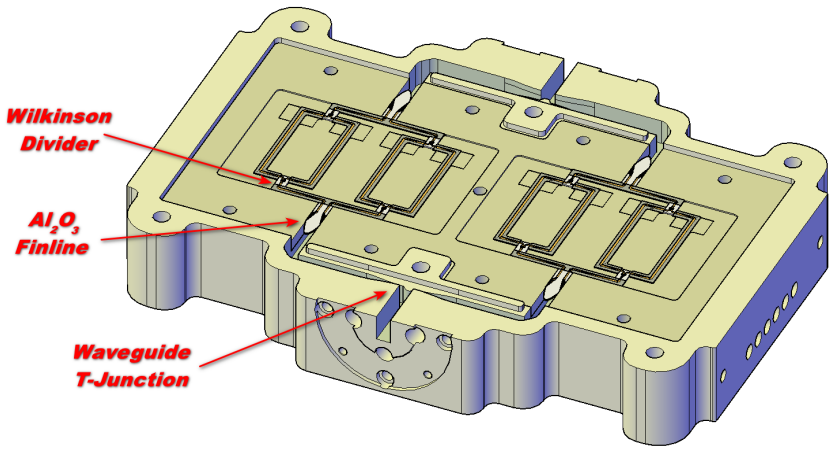

Figure 7. Passive Q-band SPC without top aluminium shell (View from mechanical drawing).

3. THERMAL SIMULATIONS

The possible applications of such a device vary from space to military. Within these environments a complete multiphysics characterization is required; therefore, electromagnetic simulation alone cannot be sufficient to certify the functioning of these systems. This is a device that will have to dissipate a considerable amount of power in the form of heat, and it must do it within a very restrictive environment, such as the satellite payload. Thermal simulation is undoubtedly the most critical and decisive design step. The passive SPC prototype realized is not required to dissipate any power, since it is possible to test it with only a network analyzer, and the measurements are intended to validate the effectiveness of the power combination technique. Since the passive structure is almost identical to the active one, with the only difference that it does not have MMICs installed, it is possible to perform thermal simulations of the final Spatial Power Amplifier, by inserting an accurate thermal model of the solid state power amplifiers into the passive system and using a multiphysics simulation software. For this project the software involved for the thermal simulations was *Ansys Mechanical* [27], and this phase started with defining the thermal model of the MMIC chosen for the final active structure, in this case the OMMIC CGY2651UH/C1. According to the data sheet of the chip, the size of this MMIC is 3.6 mm × 2.8 mm × 0.1 mm, and it is made by silicon. This is the substrate material of the device, while the channels of the field effect transistors are made by GaN (Gallium Nitride). Once the box that schematizes the chip is drawn, the next step is to model the power distribution inside the amplifier. To do this, several parallelepipeds are drawn, whose purpose is to emulate the channels of the FET devices, which are the spots at higher temperature inside the chip. In this case, only the final stage and the last driver stage were modeled since those are the areas where most of the power is dissipated (Figure 8).

The final stage is modeled as a parallelepiped of size 2 mm × 0.12 mm × 0.010 mm, while the driver stage is modeled as a parallelepiped of size 0.22 mm × 0.12 mm × 0.010 mm. These parallelepipeds are GaN material, while the rest is silicon. The final stage dissipates a DC power of 27 W, while the driver stage dissipates a DC power of 10 W. This is a good approximation of the real power sources, as a compromise among numeric computational effort, accuracy, and available data for CGY2651UH/C1. In fact, from the MMIC datasheet the DC power requirements at 40.5 GHz are a drain current of 2.7 A at 12 V, with a power output of 40 dBm. This corresponds to a drain efficiency of nearly 27%, which is a little lower than the typical PAE value of 30% given in the datasheet. So, it is possible to consider this thermal simulation as a worst-case result, i.e., when the MMICs are working at maximum RF power, they have a smaller efficiency respect to their typical value given in the datasheet.

Each MMIC is brazed on a Copper-Diamond (CuD) heat spreader with 0.508 mm thickness, and the whole assembly is glued on the copper carrier using Loctite Ablestik Ssp2020, as shown in Figure 9. A constant temperature of 50°C is considered applied at the bottom of the SPA, displayed in Figure 10, and here is where the device is anchored to the satellite cold plate.

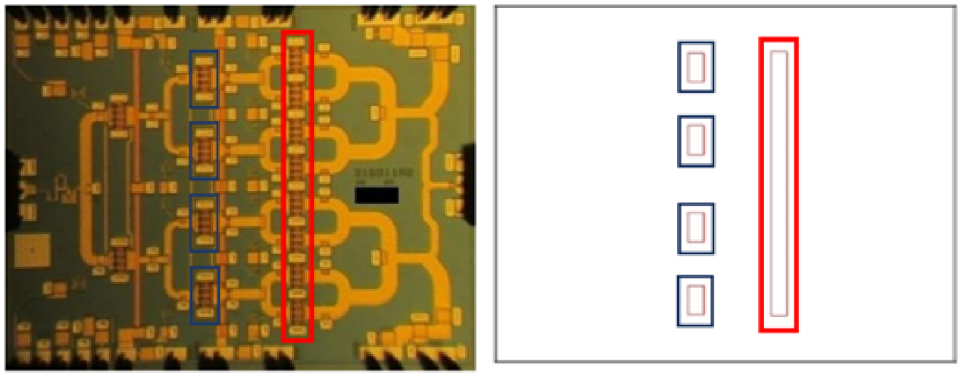

(a) (b)

Figure 8. (a) OMMIC CGY2651UH/C1 die layout and (b) model for thermal simulations.

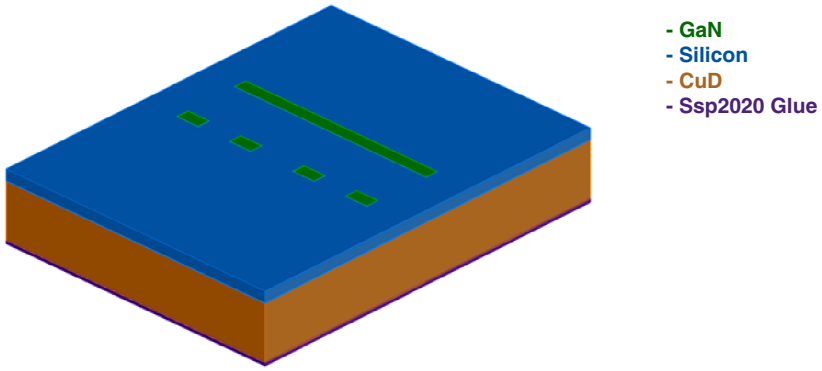

Figure 9. 3D drawing of thermal MMIC model brazed on heat spreader.

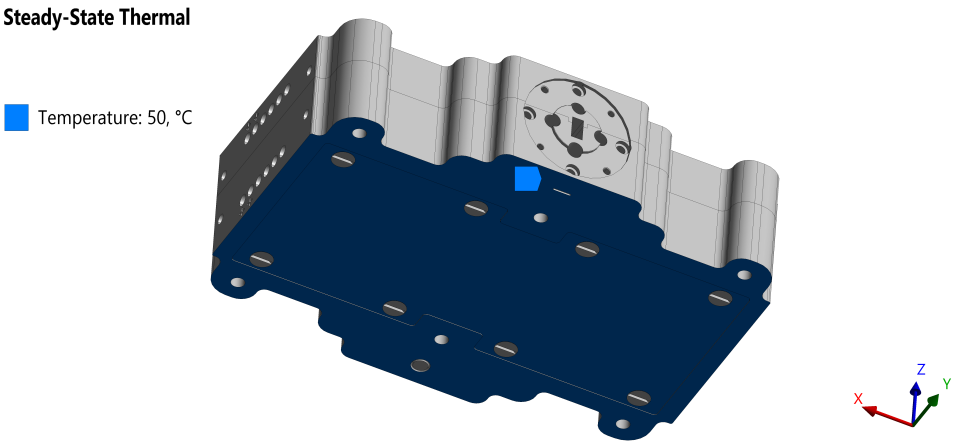

Figure 10. Constant temperature surface applied at the bottom of the SPA.

Other boundary conditions defined inside the simulator is a wider air box, with no forced air and with the external faces thermally isolated, within which the SPA is placed. The temperature distribution inside the volume of the system and along the line where the MMICs are disposed is shown Figure 11 and Figure 12.

The results shown in Figure 13 show how the passive prototype realized for this paper can withstand

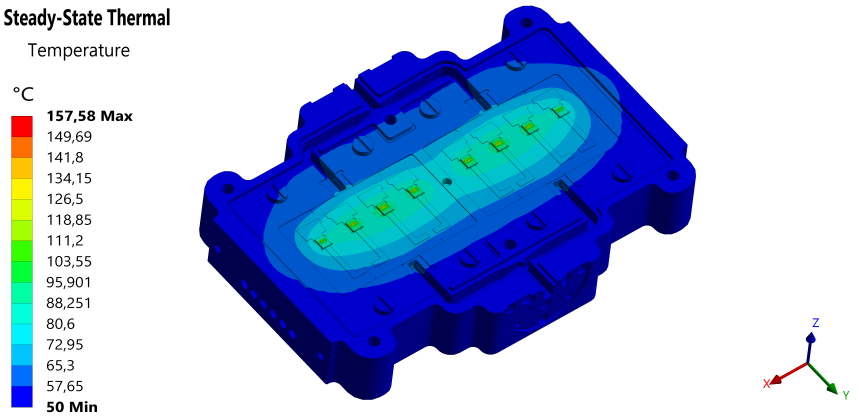

Figure 11. Temperature in the SPA volume and close to the MMICs.

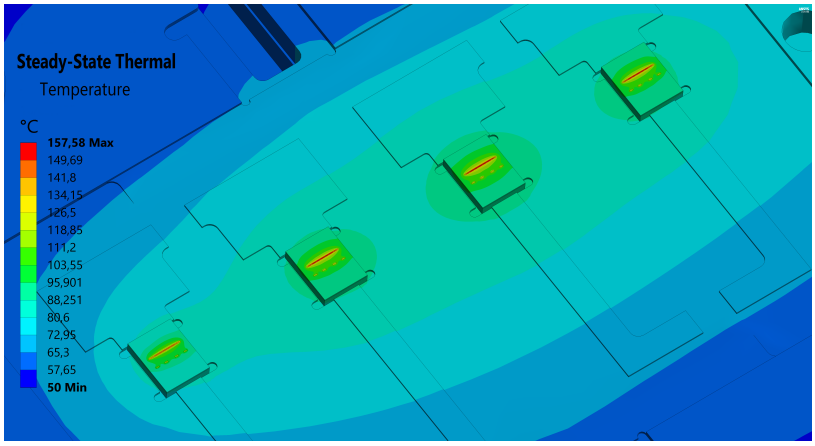

Figure 12. Temperature in the SPA volume and close to the MMICs.

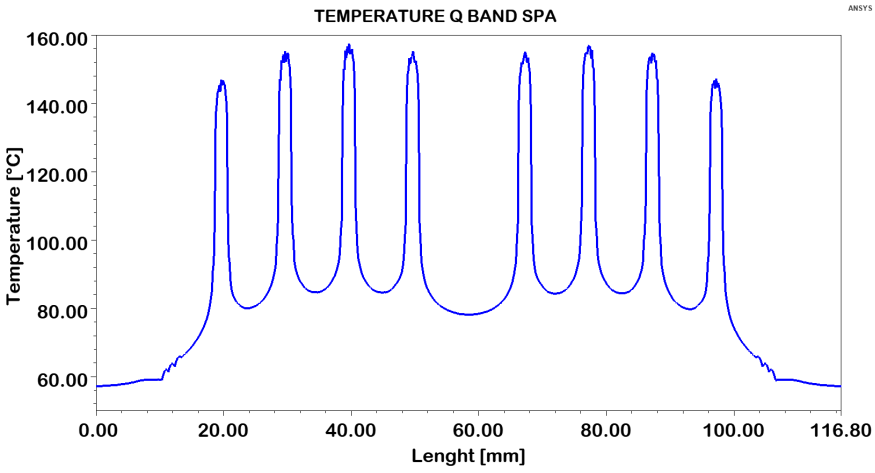

Figure 13. Temperature pattern along the MMIC stage.

the temperatures reached in case of active device operating in saturation region. In fact, the maximum temperature simulated is about 158°C, and the specification required in case of space application for European missions is 160°C.

4. STRUCTURAL MECHANICAL SIMULATIONS

Another important characterization at multiphysics level concerns the static structural aspect. In particular, the most important characteristic to be analyzed regards the ability of the structure to present minimal deformations when the entire system is subject to vibrations. This type of analysis is obviously required in avionic or satellite applications. For the latter, the vibrations of greater intensity are experienced during the launch phase of the payload. Also these simulations were performed using *Ansys Mechanical*.

The first step of the structural simulation consists in anchoring the combiner to a static support, emulating what will be its positioning inside the satellite or the aircraft; once these boundary conditions are imposed, it is necessary to calculate the mechanical resonance eigenfrequencies of the structure. For the Q band SPC proposed in this work, the first eigenfrequency occurs above 7 kHz, and other ones have been presented and plotted, up to the frequency of 10 kHz. This value represents the maximum frequency value experienced during the acceptance and qualification tests of a satellite module, and in particular, it occurs during the so-called pyrotechnic shock test in which the module must resist the shock waves caused by explosives during the launch phase. In fact, during this phase the satellite module is subject to the most critical vibrations. In terms of simulations, the forces exerted by these vibrations on the satellite components are induced by harmonic oscillations, with an acceleration module equal to a maximum of 25 g over each axis.

Thus, after anchoring the spatial power combiner and after the calculation of its mechanical resonance frequencies, harmonic accelerations with a module of 25 g are applied in order to simulate and verify the structural stability of the entire system.

The eigenfrequencies list, up to the value of 10 kHz, is shown in Table 2. In Figure 14 instead, a view of the total deformation occurs at one of the resonant modes.

Table 2. Mechanical eigenfrequencies.

Resonant Mode	Frequency [Hz]
1	7680,1
2	8028,3
3	8685,5
4	8857,4
5	9051,8
6	10241
7	10352
8	10908

Regarding a Spatial Power Amplifier, the critical deformation region is located upon the copper carrier and affects the solid state power amplifiers. In fact, if the carrier exceeds a certain deformation threshold, the MMICs will break, and since they have a thickness of 0.1 mm, they cannot be subject to the typical deformation values of classic mechanical structures.

The maximum deformation of the Q band combiner occurs around a mechanical frequency of 8.6 kHz and causes a carrier distortion of not even 2 µm along the Z axis (Figure 15), thus a more than acceptable value since the MMIC would have to undergo a deformation of only 2% of its thickness.

Drawing a line on the X axis, which crosses the center of the carrier along the Y axis, the pattern of the vertical deformation is shown in Figure 16.

Regarding the mechanical stress suffered when vibrations occur, the von-Mises stress refers to the maximum distortion criterion in the case of ductile materials, so it is the most critical type of stress in these analyses and then the most important one to evaluate.

Also in this case, the component subject to the greatest stress is the carrier, showing a maximum stress applied of 7.6 MPa, occurring at 8.6 kHz. This stress distribution is reported in Figure 17. The

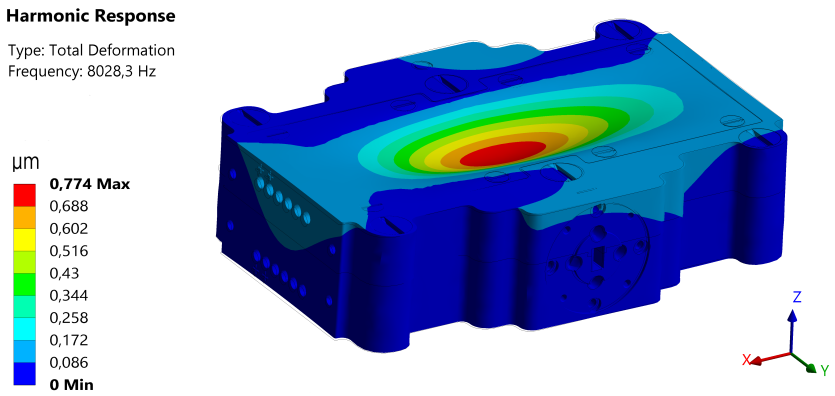

Figure 14. Total deformation plot on second resonant mode (Deformation effects are magnified for better visualization).

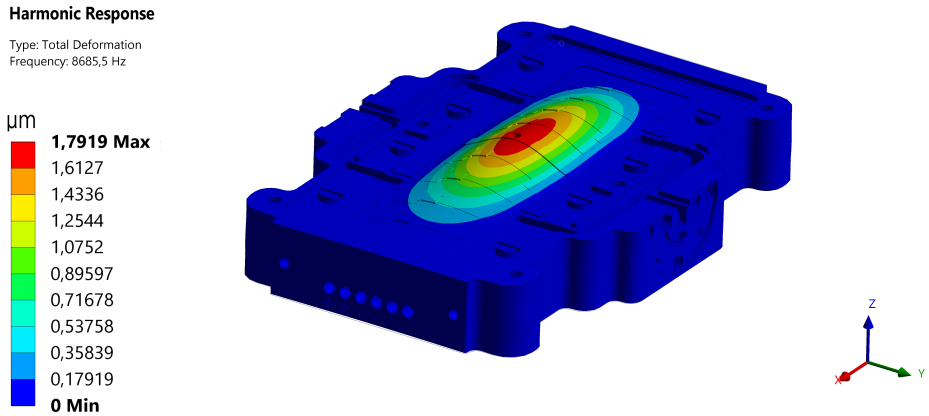

Figure 15. Maximum carrier deformation occurred at 8.6 kHz (Deformation effects are magnified for better visualization).

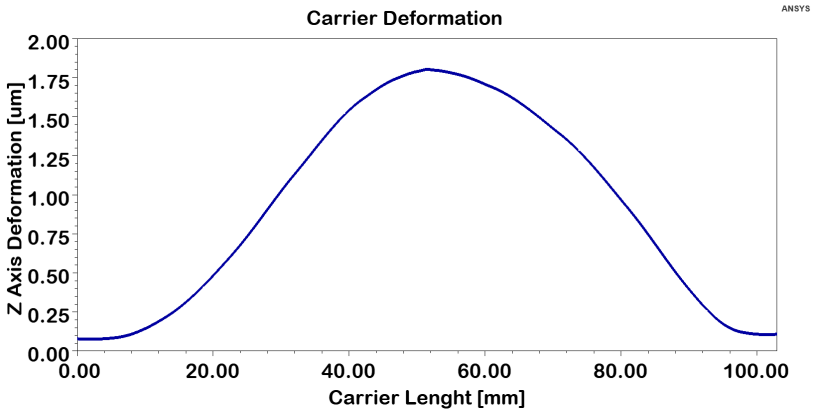

Figure 16. Module of the copper carrier deformation.

tensile strength is the maximum stress that a material can withstand before breaking, and since copper tensile strength is equal to 220 Mpa, there is no chance that the carrier will suffer any damage.

Thus, according to all the previous results, the passive Q-band SPC is ready to be completed with solid state power amplifiers, obtaining a Spatial Power Amplifier operating in Q band only adding the

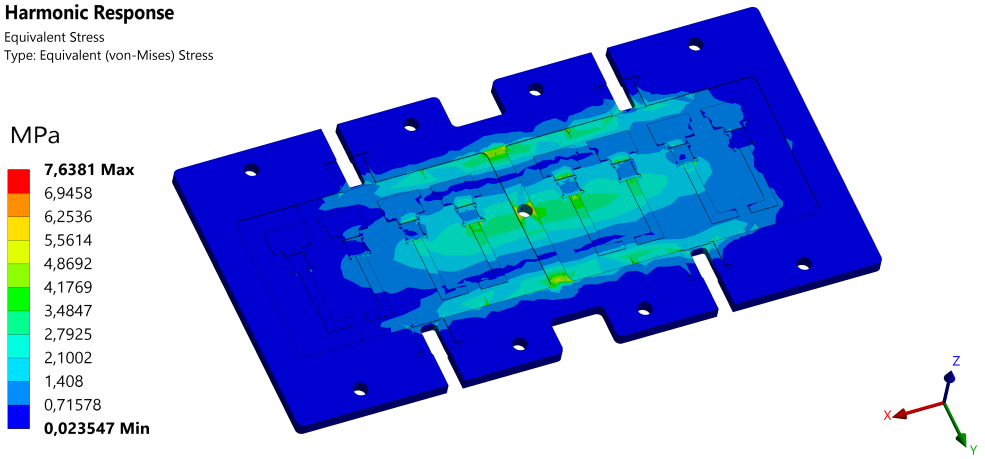

Figure 17. Distribution of Von-Mises stress over the copper carrier.

MMIC devices and without changing any other components.

For this work, the passive structure was realized, and since there is no power amplification because of the lack of the solid state power amplifiers, these types of electromagnetic structures are known in literature as Spatial Power Combiners.

5. PROTOTYPE AND MEASUREMENTS

The Q-band Spatial Power Combiner was designed by the University of Rome "Tor Vergata" following all the assumptions and the considerations mentioned above. The prototype instead was manufactured by MITEC-Roma.

The realized combiner is an aluminum box whose dimensions are $85\,\text{mm} \times 115\,\text{mm} \times 30\,\text{mm}$, and the shape of the external contours is due to the choice of reducing the system weight as much as possible, especially in the case of installation on space modules. The final weight is around 500 g which is very remarkable, and there is no other architecture capable of handling powers of hundreds of watts, in this range of frequencies and with such a low weight. The small size SPC is shown in Figure 18.

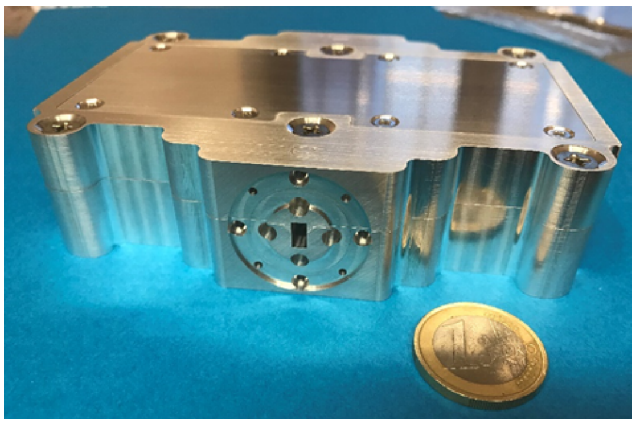

Figure 18. The measured Q-band spatial power combiner.

The test bench used for the measurements consists of a vector analyzer, two coaxial cables, and two coaxial to WR22 waveguide transitions. The whole assembled system is pictured in Figure 19. The vector analyzer is a Rohde & Schwarz zva50 with capabilities up to 50 GHz.

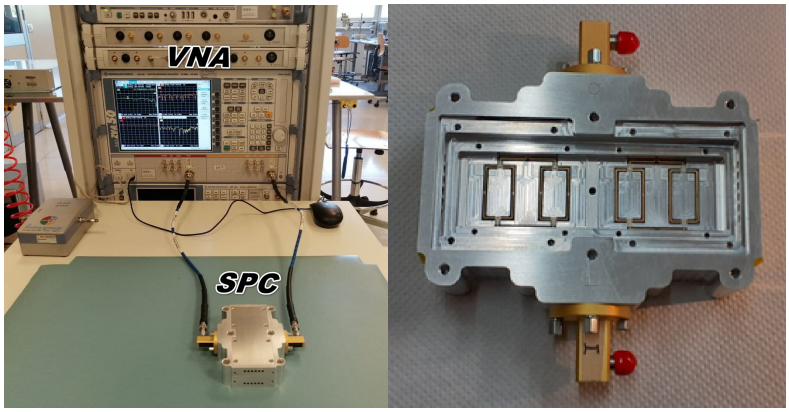

Figure 19. Q band SPC test bench and Q band SPC without the top aluminum cover.

Since the structure is passive, the only significant electromagnetic values to measure are the Return Loss and Insertion Loss, respectively S_{11} and S_{21} in terms of scattering parameters. The other two scattering parameters, S_{22} and S_{12}, are identical to the previous ones, because of the reciprocity property of a passive network [28]. These measures were carried out over the entire bandwidth covered by the WR22 waveguide, from 33 to 50 GHz, i.e., the entire Q band.

Figure 20 and Figure 21 show how the combiner presented in this paper can be matched over the whole bandwidth of the waveguide, always presenting a value below 10 dB in terms of return loss (S_{11}). Regarding the transmission losses, the bandwidth is reduced, and it is possible to consider this structure exploitable up to a frequency of 47 GHz. The mean value of insertion loss (S_{21}) shown up to this frequency is about 4 dB, but it is important to consider that this is the value of the losses between the input and output ports. In the final Spatial Power Amplifier, the important value in terms of efficiency, is the insertion loss of the path starting from the output pad of the MMICs and ending to the output waveguide port. Since the structure is symmetrical, and the solid state power amplifiers will be placed in the center of the system, it is reasonable to estimate that the output losses of the Q band Amplifier will be practically the value of this passive structure (4 dB) divided by two, and then 2 dB. With such a value of S_{21}, the Q band Spatial Power Amplifier will present a combining efficiency of 65%. Using commercial MMICs, each of them with 10 W of output power, the RF output power of the spatial amplifier will be over 100 W in the Q band spectrum, surely an impressive achievement. It is important to remark that these values are all obtained in a small volume and with an extremely low weight to power

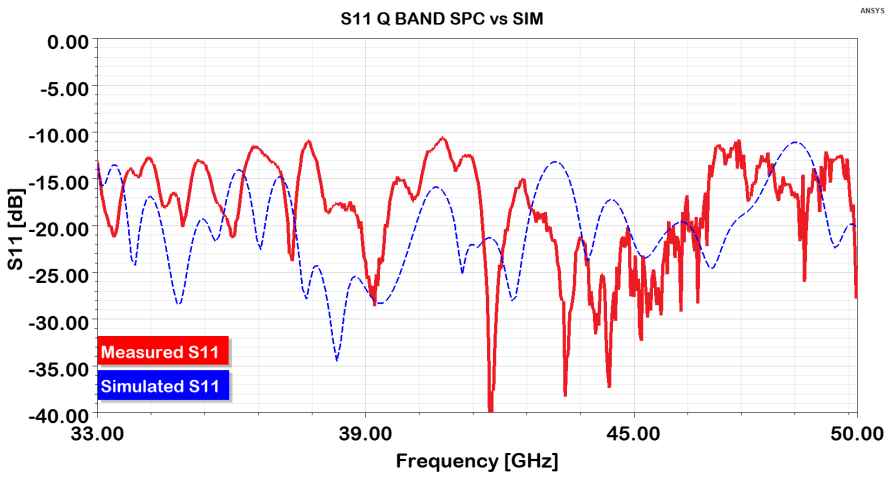

Figure 20. Return loss of Q-band SPC, measured (continuous line) and simulated (dash line).

ratio. In literature, there are structures that are more efficient in terms of combining efficiency, which are Radial Spatial Combiners; these architectures can surely reach even 80–85% combining efficiency, across this bandwidth, but the dimensions and weight are at least five times greater than the combiner presented here. Moreover, this Q band SPC can be cooled by just connecting it on a planar cool surface, such as one of the satellite walls, whereas a Radial Combiner requires a dedicated cooling system which will increase the total weight of the payload.

All these factors make Radial Combiner architectures unsuitable for space applications.

In Table 3, the performance of the structure reported in this work and the performance of the SPC amplifiers available in literature are compared. Devices operating in Q band and high Ka band are considered, and mean values of quantities are described.

Table 3. Comparison between the state of the art of SPCs in the Q band and nearest Ka band

Reference	Band GHz	Type	No. of SSPA	Output IL dB	Input RL dB	Size mm	Weight g
[29]	27–33	Circ WG	6	1.5	15	-	-
[4]	30–39.4	Rect WG	8	0.5	16	-	-
[30]	30–40	Rect WG	4	1.2	12	-	-
[31]	30–40	Circ WG	4	1.2	10	-	-
[8]	31.5–40	Rect WG	16	2.5	13	$95 \times 130 \times 23$	625
[17]	33–37	Rect WG	4	1.8	15	-	-
Proposed	33–47	Rect WG	16	2	10	$85 \times 115 \times 30$	500
[32]	42–48	Rect WG	6	0.75	10	-	-

It is important to clarify that, in the literature, very few real SPCs are available: many devices, which are identified as SPCs, are conceived to divide and combine power in the transmission line (with several losses) and use spatial combination only in the first and final stages by inserting end-launchers. However, these devices have also been reviewed in this comparison.

Despite the lack of this information, it is evident that the structure presented in this work is able to cover the widest and higher band, with the highest number of MMICs that is possible to implement, and then with the largest output power available in the case of active devices installed.

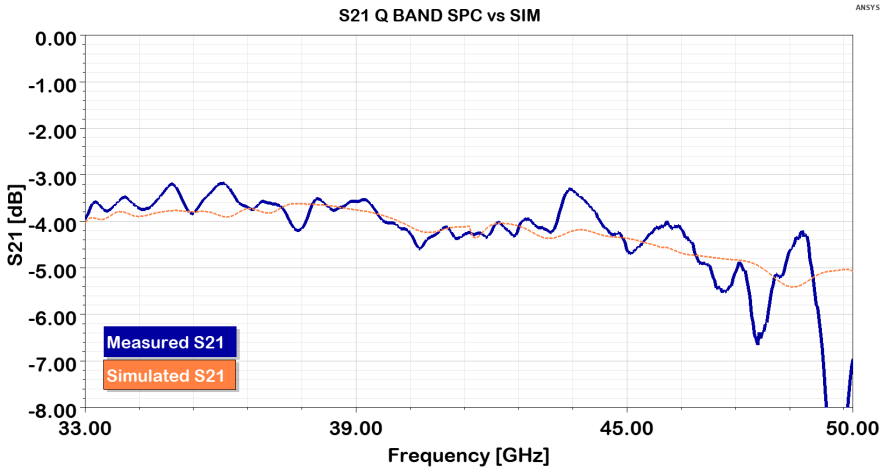

Figure 21. Insertion loss of Q-band SPC, measured (continuous line) and simulated (dash line).

6. CONCLUSION

The Spatial Power Combining structure presented in this paper is certainly the highest point reached in terms of power management at millimeter-wave frequencies. Showing a very consistent input matching, below 10 dB, and minimizing the transmission losses from 33 to 47 GHz, this Q band power combiner represents a natural solution for all the satellite applications in which a large amount of millimeter-wave power must be guaranteed. The mean value of the insertion losses is 4 dB, which can lead to an average combining efficiency of 65% once the solid state power amplifiers are added to the structure. Multiphysics simulations show how inside this aluminium box of 290 mm^3, an RF power of 100 W can be exploited, without exceeding half a kilo in weight. This is a remarkable achievement, especially in the case of geostationary satellites. Considering the growing demand from space agencies in such terms, this device will surely play a key role in future satellite payloads.

ACKNOWLEDGMENT

This work was supported by European Space Agency (ESA) through the Spatial Power Combining Amplifiers at Q/V band for Satellite Communications project in frame of the ESA ARTES Competitiveness and Growth (C&G) program.

The Authors thank ST4I (Space Technologies for Innovation srl) for the opportunity offered, Amitabh Chowdhary (ESA) and Iain Davies (ESA) for helpful discussions on technical aspects, MITEC srl for the prototype manufacturing, SDS srl for the support in measurements.

REFERENCES

1. Passi, D., A. Leggieri, F. Di Paolo, A. Tafuto, and M. Bartocci, "Spatial power combiner technology," *PIERS Proceedings*, 932–938, Prague, Czech Republic, July 6–9, 2015.
2. Passi, D., A. Leggieri, A. Mattioni, F. Di Paolo, M. D'Antoni, M. Bartocci, E. Ciacia, and A. Tafuto, "Small size, high power density, solid state amplifiers for space application," *2018 International Symposium on Networks, Computers and Communications (ISNCC)*, 1–5, 2018, doi: 10.1109/ISNCC.2018.8531030.
3. Yin, K., K. Zhang, and J. Xu, "Characterization and design of millimeter-wave full-band waveguide-based spatial power divider/combiner," *Progress In Electromagnetics Research C*, Vol. 50, 65–74, 2014.
4. Kang, Z.-Y., Q.-X. Chu, and Q. S. Wu, "A compact Ka-band broadband waveguide-based traveling-wave spatial power combiner with low loss symmetric coupling structure," *Progress In Electromagnetics Research Letters*, Vol. 36, 181–190, 2013.
5. Passi, D., et al., "Innovative transition for wideband spatial combiners," *2018 International Workshop on Integrated Nonlinear Microwave and Millimetre-wave Circuits (INMMIC)*, 1–3, 2018, doi: 10.1109/INMMIC.2018.8430013.
6. Leggieri, A., D. Passi, G. Saggio, and F. Di Paolo, "Multiphysics design of a spatial combiner predisposed for thermo-mechanically affected operation," *Journal of Electromagnetic Waves and Applications*, Vol. 28, No. 17, 2153–2168, 2014.
7. Leggieri, A., D. Passi, G. Saggio, and F. di Paolo, "Global design of a waveguide X-band power amplifier," *Int. J. Simul. Syst. Sci. Technol.*, Vol. 15, No. 4, 2014, doi: 10.5013/IJSSST.a.15.04.09.
8. Passi, D., A. Leggieri, F. Di Paolo, M. Bartocci, and A. Tafuto, "Design of high power density amplifiers: Application to Ka band," *J. Infrared, Millimeter, Terahertz Waves*, Vol. 38, No. 10, 1252–1263, 2017, doi: 10.1007/s10762-017-0402-1.
9. Leggieri, A., D. Passi, and F. Di Paolo, "The squarax amplifier: An electromagnetic and thermo-mechanical innovation," *Progress In Electromagnetics Research Symposium Proceedings*, 2273–2280, Guangzhou, China, August 25–28, 2014.
10. Leggieri, A., G. Orengo, D. Passi, and F. Di Paolo, "The squarax spatial power combiner," *Progress In Electromagnetics Research C*, Vol. 45, 43–55, 2013.

11. Passi, D., A. Leggieri, F. Di Paolo, M. Bartocci, A. Tafuto, and A. Manna, "High efficiency Ka-band spatial combiner," *Adv. Electromagn.*, Vol. 3, No. 2, 2014, doi: 10.7716/aem.v3i2.267.
12. Leggieri, A., D. Passi, F. Di Paolo, M. Bartocci, A. Tafuto, and A. Manna, "A novel Ka-band spatial combiner amplifier: Global design and modeling," *PIERS Proceedings*, 840–845, Prague, Czech Republic, July 6–9, 2015.
13. Valletti, L., S. Fantauzzi, M. Bartocci, P. Bia, A. Manna, P. Livreri, F. Di Paolo, and E. Limiti, "Vircator technologies comparison and novel anode analysis," *2021 PhotonIcs & Electromagnetics Research Symposium (PIERS)*, 2781–2789, Hangzhou, China, November 22, 2021.
14. Passi, D., A. Leggieri, R. Citroni, and F. Di Paolo, "Broadband TE10 to TE20 mode transformer for X band," *Adv. Electromagn.*, Vol. 5, No. 3, 2016, doi: 10.7716/aem.v5i3.419.
15. Passi, D., A. Leggieri, R. Citroni, and F. Di Paolo, "New six-way waveguide to microstrip transition applied in X band spatial power combiner," *Adv. Electromagn.*, Vol. 6, No. 4, 2017, doi: 10.7716/aem.v6i4.421.
16. Yin, K., J. P. Xu, and Z. H. Chen, "A full Ka-band waveguide-based spatial power-combining amplifier using *E*-plane anti-phase probes," State Key Lab. of Millimeter-waves, Southeast University, Nanjing, Jiangsu, 2014.
17. Zhou, Y.-H., J.-Y. Li, B. Zhao and H.-Y. Wang, "A Ka-band power amplifier based on double-probe microstrip to waveguide transition," *PIERS Proceedings*, 1521–1525, Xi'an, China, March 22–26, 2010.
18. Fantauzzi, S., L. Valletti, and F. Di Paolo, "Virtual prototype of innovative Ka-band power amplifier based on waveguide polarizer," *Adv. Electromagn.*, Vol. 9, No. 2, 60–65, 2020, doi: 10.7716/aem.v9i2.1497.
19. Khan, P., L. Epp, and A. Silva, "A Ka-band wide-bandgap solid-state power amplifier: Architecture performance estimates," *The Interplanetary Network Progress Report*, Vol. 42-163, 1–17, November 2005.
20. Lee, S. H., D. H. Lee, and J. H. Chang, "X-band 1 kW SSPA using 20-way hybrid radial combiner for accelerator," *2016 Asia-Pacific Microwave Conference (APMC)*, 1–4, 2016, doi: 10.1109/APMC.2016.7931274.
21. Kazemi, R., G. Hegazi, and A. E. Fathy, "X-band all-waveguide radial combiner for high power applications," *2015 IEEE MTT-S International Microwave Symposium*, 1–4, 2015, doi: 10.1109/MWSYM.2015.7166748.
22. Denoual, J. M., A. Peden, B. Della and J.-P. Fraysse, "16-way radial divider/combiner for solid state power amplifiers in the K band," *2008 38th European Microwave Conference*, 345–348, 2008, doi: 10.1109/EUMC.2008.4751459.
23. Zhai, G. and B. Shi, "Compact low loss millimeter wave 8-way radial waveguide power combiner," *TENCON 2017 — 2017 IEEE Region 10 Conference*, 1598–1601, 2017, doi: 10.1109/TENCON.2017.8228112.
24. Sarhan, A. A., N. Ghadimi, E. Hamidi, and H. Oraizi, "Broadband radial waveguide power combiner with improved isolation among adjacent output ports," *Progress In Electromagnetics Research C*, Vol. 51, 63–70, 2014.
25. Bhat, B. and S. K. Koul, *Analysis, Design and Applications of Fin Lines*, Artech House, 1987.
26. https://www.ansys.com/products/electronics/ansys-hfss.
27. https://www.ansys.com/products/structures/ansys-mechanical.
28. Di Paolo, F., *Networks and Devices Using Planar Transmission Lines*, CRC Press, 2000.
29. Xu, J., Y. Cui, C. Qian, and W. Li, "A Ka-band power-combined amplifier based on a six-way quasi-planar power divider/combiner," *2015 Asia-Pacific Microwave Conference (APMC)*, 1–3, 2015, doi: 10.1109/APMC.2015.7411821.
30. An, D., X. Li, J. Mou, and X. Lv, "A new type of ka-band waveguide-based power-combining structures," *2008 International Conference on Microwave and Millimeter Wave Technology*, 347–350, 2008, doi: 10.1109/ICMMT.2008.4540383.

31. Yin, K., "Millimeter wave power-combined amplifier using traveling-wave power divider-combiner," *2015 Asia-Pacific Microwave Conference (APMC)*, 1–3, 2015, doi: 10.1109/APMC.2015.7413379.
32. Xu, J., Z. Xu, J. Guo, H. C. Zhang, C. Qian, and D. Zhao, "Design of a Q-band six-way spatial power combining structure," *2018 IEEE MTT-S International Wireless Symposium (IWS)*, 1–3, 2018, doi: 10.1109/IEEE-IWS.2018.8400955.